Brain and Spine 4 (2024) 102813

Contents lists available at ScienceDirect

Brain and Spine

journal homepage: www.journals.elsevier.com/brain-and-spine

A 72-h sedated porcine model of traumatic spinal cord injury

Mathias Møller Thygesen [a,b,c,*], Seyar Entezari [a,b,c], Nanna Houlind [a,b,c], Teresa Haugaard Nielsen [a,b,c], Nicholas Østergaard Olsen [a,b,c], Tim Damgaard Nielsen [a,b,c], Mathias Skov [c], Joel Borgstedt-Bendixen [a], Alp Tankisi [d], Mads Rasmussen [d], Halldór Bjarki Einarsson [a], Peter Agger [c], Dariusz Orlowski [a], Stig Eric Dyrskog [e], Line Thorup [e], Michael Pedersen [c], Mikkel Mylius Rasmussen [a,b]

[a] Department of Neurosurgery, Aarhus University Hospital, Denmark
[b] Department of Clinical Medicine CENSE, Aarhus University, Denmark
[c] Department of Clinical Medicine Comparative Medicine Lab, Aarhus University, Denmark
[d] Department of Anesthesiology, Aarhus University Hospital, Denmark
[e] Department of Intensive Care, Aarhus University Hospital, Denmark

ARTICLE INFO

Handling editor: F Kandziora

Keywords:
Traumatic spinal cord injury
Translational animal model
Critical care model
Diffusion magnetic resonance imaging

ABSTRACT

Introduction: There is an increasing focus on the prevention of secondary injuries following traumatic spinal cord injury (TSCI), especially through improvement of spinal cord perfusion and immunological modulation. Such therapeutic strategies require translational and controlled animal models of disease progression of the acute phases of human TSCI.
Research question: Is it possible to establish a 72-h sedated porcine model of incomplete thoracic TSCI, enabling controlled use of continuous, invasive, and non-invasive modalities during the entire sub-acute phase of TSCI?
Material and methods: A sham-controlled trial was conducted to establish the model, and 10 animals were assigned to either sham or TSCI. All animals underwent a laminectomy, and animals in the TSCI group were subjected to a weight-drop injury. Animals were then kept sedated for 72 h. The amount of injury was assessed by ex-vivo measures MRI-based fiber tractography, histology and immunohistochemistry.
Results: In all animals, we were successful in maintaining sedation for 72 h without comprising vital physiological parameters. The MRI-based fiber tractography showed that all TSCI animals revealed a break in the integrity of spinal neurons, whereas histology demonstrated no transversal sections of the spine with complete injury. Notably, some animals displayed signs of secondary ischemic tissue in the cranial and caudal sections.
Discussion and conclusions: This study succeeded in producing a porcine model of incomplete TSCI, which was physiologically stable up to 72 h. We believe that this TSCI model will constitute a potential translational model to study the pathophysiology secondary to TSCI in humans.

1. Introduction

The primary mechanical insult of traumatic spinal cord injury (TSCI) causes permanent damage to the spinal cord. Furthermore, the mechanical forces initiate a cycle of secondary pathophysiological effects. These effects include a paradoxical immunological injury caused by exposure of the spinal cord to the systemic immunological system (Silver et al., 2015; Schwab et al., 2014; Popovich et al., 1999; Kigerl et al., 2009); and spinal cord hypoperfusion caused by the swelling of the spinal cord, and development of a subdural compartment syndrome (Werndle et al., 2013; Saadoun et al., 2016, 2020; Tator et al., 1991).

While the primary injury is beyond therapeutic grasp, the secondary pathophysiological effects seem modulable by decompression of intraspinal pressure (Phang et al., 2015), augmentation of spinal blood

* Corresponding author. Department of Clinical Medicine Comparative Medicine Lab, Aarhus University, Denmark.
E-mail addresses: matthy@clin.au.dk (M.M. Thygesen), seyent@clin.au.dk (S. Entezari), nahoul@rm.dk (N. Houlind), teresa@clin.au.dk (T.H. Nielsen), 201709605@post.au.dk (N.Ø. Olsen), tidani@rm.dk (T.D. Nielsen), skov.mathias@biomed.au.dk (M. Skov), joel.bakke@rm.dk (J. Borgstedt-Bendixen), alptanki@rm.dk (A. Tankisi), mads.rasmussen@vest.rm.dk (M. Rasmussen), h.einarsson@rn.dk (H.B. Einarsson), peter.agger@clin.au.dk (P. Agger), dorl@clin.au.dk (D. Orlowski), Stig.Dyrskog@rm.dk (S.E. Dyrskog), Line.Thorup@vest.rm.dk (L. Thorup), michael@clin.au.dk (M. Pedersen), mikkrasm@rm.dk (M.M. Rasmussen).

https://doi.org/10.1016/j.bas.2024.102813
Received 9 October 2023; Received in revised form 20 December 2023; Accepted 17 January 2024
Available online 16 April 2024

perfusion (Saadoun et al., 2020; Thygesen et al., 2021) and suppression of the paradoxical immunological cascade (Silver et al., 2015; Schwab et al., 2014; Gee et al., 2022; Squair et al., 2019; Phang et al., 2014). Nevertheless, these interventions are most likely only relevant in incomplete TSCI.

Human studies disallow sampling of spinal cord tissue, invasive parenchymal monitoring and aggressive interventions. Thus, there are numerous advantages in using animals as models of TSCI. However, successful interventions in animal models have often failed translation into the Clinic (James et al., 2015; Zorner et al., 2010), possibly due to

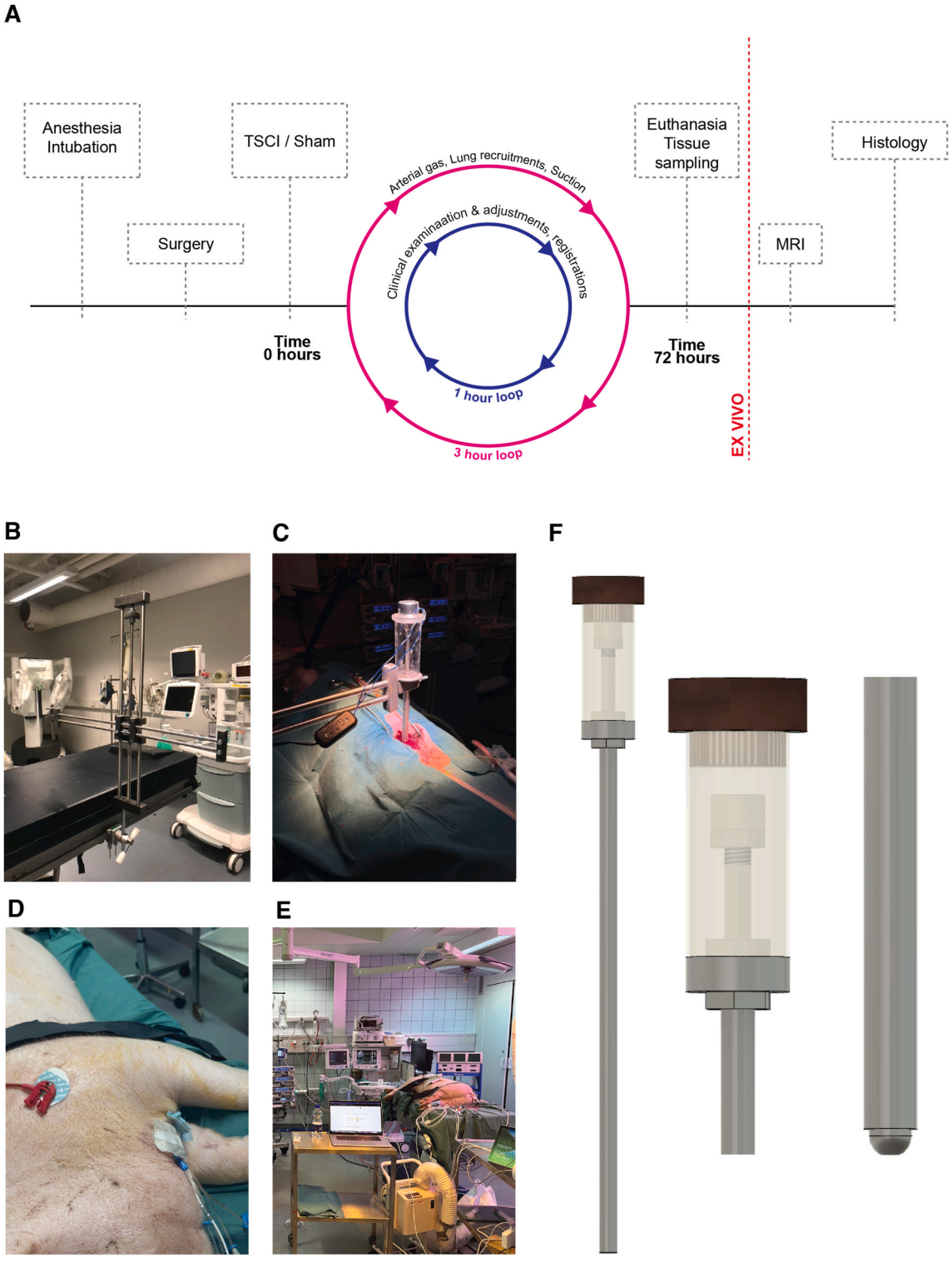

Fig. 1. Methods f. (A) Timeline depicting the overall progress through the study. The loops are representative of the one- and 3-h repeating measures and interventions. (B) Photo of the moving arm connected to the surgical table. (C) The trauma device during the study. The photo is taken just prior to release of the rod. (D) Overview of the operating room/intensive care. Photo shows the ventilator, pumps and monitoring. The photo is taken just after surgery. (E) The jugular central venous line. (F) 3D rendered model of the trauma device. On the left the entire system is shown, with the rod held in place by the electromagnet. In the center the release of the rod is show. On the right the protrusion of the rod through the cylinder is shown.

the discrepancies in size, neuroanatomy and neuroimmunological responses to TSCI that exist between human and animals, particularly in studies using rodents and other small-sized species. This concern has been the primary motivation for establishing multiple large animal models, particularly in pigs that share several physiological, anatomical and immunological characteristics to humans (West et al., 2020a; Streijger et al., 2017; Cerro et al., 2021; Martirosyan et al., 2015; Weber-Levine et al., 2022; Schomberg et al., 2017). However, most studies with TSCI animal models have been performed with short-term sedations (West et al., 2020b; Streijger et al., 2018a), (few hours) or as survival models with awake animals (several days) (Streijger et al., 2017, 2021; Cerro et al., 2021). These models benefit from opportunities to receive long-term data, but they also must cope with influences from movement, animal behavior, risk of probe displacement, and therefore less rigor in physiological monitoring and modulation. Hence, there is a lack of sedated, non-moving and highly controlled animal model, allowing studies of precise physiological measurements of the entire sub-acute period following onset of TSCI.

In this study, we aimed to establish a 72-h sedated porcine model of TSCI to study the acute phase response in a strictly controlled environment. We hypothesized that an incomplete contusion thoracic TSCI could be produced by a weight-drop procedure and that the animal could be kept physiologically stable during the entire study period.

2. Materials and methods

2.1. Study design and overall setup

The study was designed as a randomized trial between a low thoracic TSCI intervention and a sham surgery. All animals underwent surgery and from infliction of injury kept sedated for 72 h, before being euthanized (Fig. 1A). The spinal cords were sampled for ex-vivo examinations. The injury was inflicted by a developed weight drop device (Fig. 1B and C).

2.2. Animals

Female Danish Landrace pigs weighing 38–42 kg were used. The study was approved by the Danish Animal Research Inspectorate (no. 2020-15-0201-00687).

2.3. Anesthesia and analgesia

On the day of the experiment, the animal was fasted for 6 h and received a preanesthetic intramuscular injection of Zoletil Vet 50 (Virbec, Carros, France). Peripheral intravenous catheters were placed, before intubation (6.5 mm, cuffed endotracheal tube) and start of mechanical ventilation.

Under aseptic conditions and using ultrasonography, a central 5-lumen venous catheter (Fig. 1D) and arterial line were placed in the jugular vein and the posterior tibial artery respectively.

2.4. Infusion strategy

We applied a clinically guided anesthetic regime in contrast to a dose standardized regime. Hence, we decided to standardize sedation depth rather than infusion rates. The animal received an initial infusion of 12 mL/h of propofol (10 mg/mL Propofol B, Braun), 12 mL/h of fentanyl (50 μg/mL Fentanyl, Hameln) and 4 mL/h of midazolam (1 mg/mL Midazolam, Hameln). If anesthesia was judged insufficient from examination of central reflexes, and or reaction to stimuli, the infusion rates of propofol and midazolam were increased adequately in a 2:1 relation, meaning that for each 2 mL/h of increase in propofol, midazolam was increased by 1 mL/h. Upon increasing the infusion rate, a bolus of 1–4 mL of propofol and/or 1–4 mL of midazolam was administered, depending on the current infusion rate and subsequent physiological effect.

2.5. Ventilation strategy

Mechanical ventilation was adjusted to maintain blood gas measures within normal ranges. Volume-controlled ventilation modulus was used, and startup settings included tidal volume of 400 mL (1 mL/kg), respiratory rate of 12 per min, and peak end expiratory pressure (PEEP) of 5 cmH_2O.

2.6. Intensive care protocol and reference ranges for physiological parameters

The animal was kept sedated mimicking the procedures at intensive care units (ICU) (Fig. 1E). The animal was constantly being overseen by trained personnel (doctors and/or medical students). Every hour, values from the intensive care monitor and the ventilator were manually registered and the animal was clinically examined for reflexes and reactions to stimuli. Furthermore, monitor data (Philips Intellivue MX500) were logged continuously using ICM+ (University of Cambridge) (Smielewski et al., 2005). Arterial blood gasses were obtained every 3 h. If deemed necessary, adjustments to medications and/or ventilation were performed as described below. All reference ranges are were based on the work of Hannon et al. (Table 1) (Hannon et al., 1990).

To ensure adequate ventilation and reduce airway pressure, lung recruitment and suction were performed every 3 h for the entire course of the experiment. PEEP was increased to a maximum of 8 cmH_20, if judged necessary, due to increasing airway pressures.

Hypotension was treated by infusion of norepinephrine when mean arterial blood pressure (MAP) fell below 65 mmHg for 5 min. Hypertension was not treated. The temperature was regulated by using a hot air blanket, aiming for the range of 38–39 °C. A volume of 750 mg of cefuroxime was administered every 8 h. Potassium chloride was administered when blood levels of potassium were below 3.5 mmol/L.

The animal was positioned in the recumbent position after surgery, changing between right and left, every morning at approximately 8 a.m. All intravenous catheters were flushed 3 h. A urine catheter was placed before surgery and fluid balance was assessed 1 h, registering in- and output. Urine output was aimed to be at 1–2 mL/kg/h. A gastric feeding tube was used to start an infusion of 40 mL/h of enteral nutrition (Nutricia Nutrison Protein Plus).

2.7. Surgical procedure

The midpoint of the surgical level was defined as follows: four vertebrae above the most caudal rib, corresponding to thoracic level 8. A midline incision was performed and subsequent subperiosteal dissection of the paravertebral musculature and a 2.5 level laminectomy was performed. The width of the laminectomy was adjusted to the falling rod (see below).

Table 1
Reference values for the experiments. The values are based on the work by Hannon et al. MAP: Mean arterial pressure, HR: Heart rate, Hgb: hemoglobin.

	Reference range	
MAP [mmHg]	65.00	.
HR [c/m]	40.00	100.00
Temperature [°C]	38.00	39.00
pH	7.40	7.53
pO2 [kPa]	9.73	.
pCO2 [kPa]	4.50	5.90
glucose [mmol/L]	2.60	6.50
Hgb [mmol/L]	4.53	6.33
Sodium [mmol/L]	129.00	143.00
Potassium [mmol/L]	3.50	5.00
Chloride [mmol/L]	93.00	126.00
Urine output 1 h [mL]	40.00	80.00

For sham animals, the surgical incision was closed. For the TSCI animals, the weight drop injury was now inflicted, and following the wound was closed in three layers (fascia, subcutaneous, and skin). No wound drainage was used. In the case of epidural bleeding, hemostasis was obtained using fibrillar (Surgicel) or surgiflo (Ethicon).

2.8. Injury protocol and weight-drop device

The injury was inflicted by a custom-made weight-drop device using a 75 mm fall of a 75 g round tipped rod. The cylinder was kept in place on the spinal cord, producing sustained compression, for 5 min. The design was a falling rod within a cylinder (Fig. 1F). The rod diameter was 7.5 mm. The falling height (75 mm) was defined by a cylinder spacer. The rod was held by an electromagnet connecting to the magnetic top of the rod. The rod is released after turning off the electromagnet, ensuring no touch during release. The rod was 5 mm longer than the cylinder with a rounded tip (5 mm radius). The laminectomy was the width of the rod, ensuring that the cylinder would just rest on the facet joints and remaining laminae. The cylinder was lowered to a position just posterior to the dura, before releasing the falling rod. The entire system was kept in place by a custom-made moving arm mounted to the surgical table (Fig. 1B), allowing for precise placement of the cylinder.

2.9. Tissue sampling

At 72 h after injury/end of surgery (sham group), the surgical wound was reopened, and the dura was exposed. Before transecting and removing the spinal cord, the animal was euthanized using pentobarbital. Following, the spinal cord was excised immediately after, and immersion-fixated in 4% formaldehyde solution.

2.10. MRI diffusion tensor imaging and tractography

Ex-vivo MRI diffusion tensor imaging (DTI) scans were performed on the fixated samples. The samples were scanned in two batches. Samples were scanned using a DTI sequence, using 30 diffusion directions, isotropic resolution of $0.5 \times 0.5 \times 0.5$ mm^3,4 averages, echo-time: 27 ms, repetition-time: 7099 ms, an acquisition time of 51 h.

Scans were masked using a manually constructed mask before postprocessing (Thermo Scientific Amira Software). MRtrix3 was used for computing the tractography (Tournier et al., 2019) using the Tensor Deterministic Algorithm with the settings of: 10.000 seeding points per sample, an angle threshold of 35°, and a fractional anisotropy (FA) threshold of 0.23. The Tensor Deterministic Algorithm was only allowed to seed within the mask, hence within the tissue.

The FA threshold was determined by computing the normal range of FA value in our dataset by: First; segmenting the white matter of sham spinal cords, second; computing the lower bound of the 95% prediction interval for each animal, and third; computing the mean of the lower bounds across all sham animals, yielding the mean 95% predictions lower bound (0.23).

A fixed number of tracts were not used, as it would result in an underestimation of tracts in the injured samples and an overestimation in the non-injured.

In the most cranial part of the scan, a rectangular region of interest (ROI), was placed spanning the entire transverse section of each spinal cord. The number of tracts traversing this ROI was counted. Then two ROIs at 5 and 10 mm from the first were placed, and the number of the tracts from the first to the second and third ROIs were counted respectively.

2.11. Histology

After a minimum of two weeks of fixation, the samples were cryoprotected in a 30% sucrose in phosphate-buffered saline solution for 7–10 days. For sectioning the samples were then frozen in isopentane cooled by dry ice and sectioned into 40 μm thick sections. The section interval was 1 mm. Five sections from the cranial, epicenter, and caudal part of the sample were withdrawn for each stain. Sections were mounted directly on the slides. Nissl stain was used to visualize morphological changes in the tissue. Macrophages and microglia were visualized by immunohistochemistry, using rabbit anti Ionized calcium binding adaptor molecule-1antibody (IBA1) (WAKO, 019–19741, 1:1000) followed by incubation with the secondary goat anti-rabbit antibody (Abcam, ab6720, 1:200). Astrocytes were visualized using immunohistochemistry, using mouse monoclonal anti-GFAP antibody (Abcam, ab4648, 1:2000) followed by incubation with goat anti-mouse antibody (DAKO 1:200).

White matter was visualized by immunohistochemistry using a mouse anti-myelin basic protein (MBP) antibody (Biolegend, 836504, 1:300) followed by incubation with the goat anti-mouse antibody (Abcam, ab97033, 1:200). All immunohistochemical sections were visualized using ABC Vectastain and DAB reaction, dehydrated in 99% ethanol, and mounted using Pertex medium.

Qualitative evaluation was performed using a microscope and scanned slides. Quantitative evaluation was performed using ImageJ (Schindelin et al., 2012). White matter injury was defined as areas of decreased Nissl-staining and for the grey matter a lack of visible nuclei, or tissue displaying histological changes which could not be attributed to artifacts. A ROI was drawn around the entire cord, and then another for the injured area. The ratio between the injured and total areas were then computed for each section.

2.12. Statistics

For each physiological parameter, the mean and the proportion of measurements outside the reference range were computed, for each animal. The mean proportion of each group was then compared. Means are presented with 95% Confidence intervals in square brackets, unless otherwise stated.

The number of tracks seeding from the cranial ROI and reaching the caudal ROI was compared between groups. The mean FA-value at the epicenter of the injury was compared.

Non-parametric bootstrapped (10000 repetitions) *t*-test was used, due to the low number of replicates in each group. All analyses were performed using Stata 17 (StataCorp. 2021. Stata Statistical Software: Release 17. College Station, TX: StataCorp LLC).

3. Results

Thirteen animals were planned. Two animals were excluded due to severe illness upon arrival at the labs. Eleven animals were included in the study, five sham animals and six TSCI animals.

3.1. DTI - tractography and FA

One animal was not scanned, hence only 10 animals were eligible for DTI analysis. The QQ-plot found the track count and FA values of the TSCI animals, to be slightly skewed, and as such a bootstrapped *t*-test was used to evaluate the difference between groups.

The tractography algorithm was successful in seeding a mean of 5123 [2467, 7780] tracks at the cranial end of each sample in the sham group, whilst a mean of 2240 [1010, 3471] tracks for each sample in the TSCI group (Fig. 2A). In the sham group a mean of 4812 [2179, 7445] tracks reached the caudal end of the sample, whereas for the TSCI group a mean of 772 [−294, 1837] reached the caudal end (Fig. 2A). The mean difference between groups in tracks reaching the caudal end was 4040 [2142, 5939] and reached statistical significance ($p < 0.000$) (Fig. 2A). The algorithm was successful in tracking injury-traversing tracts for all animals (Fig. 2B).

The mean FA-value at the epicenter ROI was 0.52 [0.48, 0.57] for the

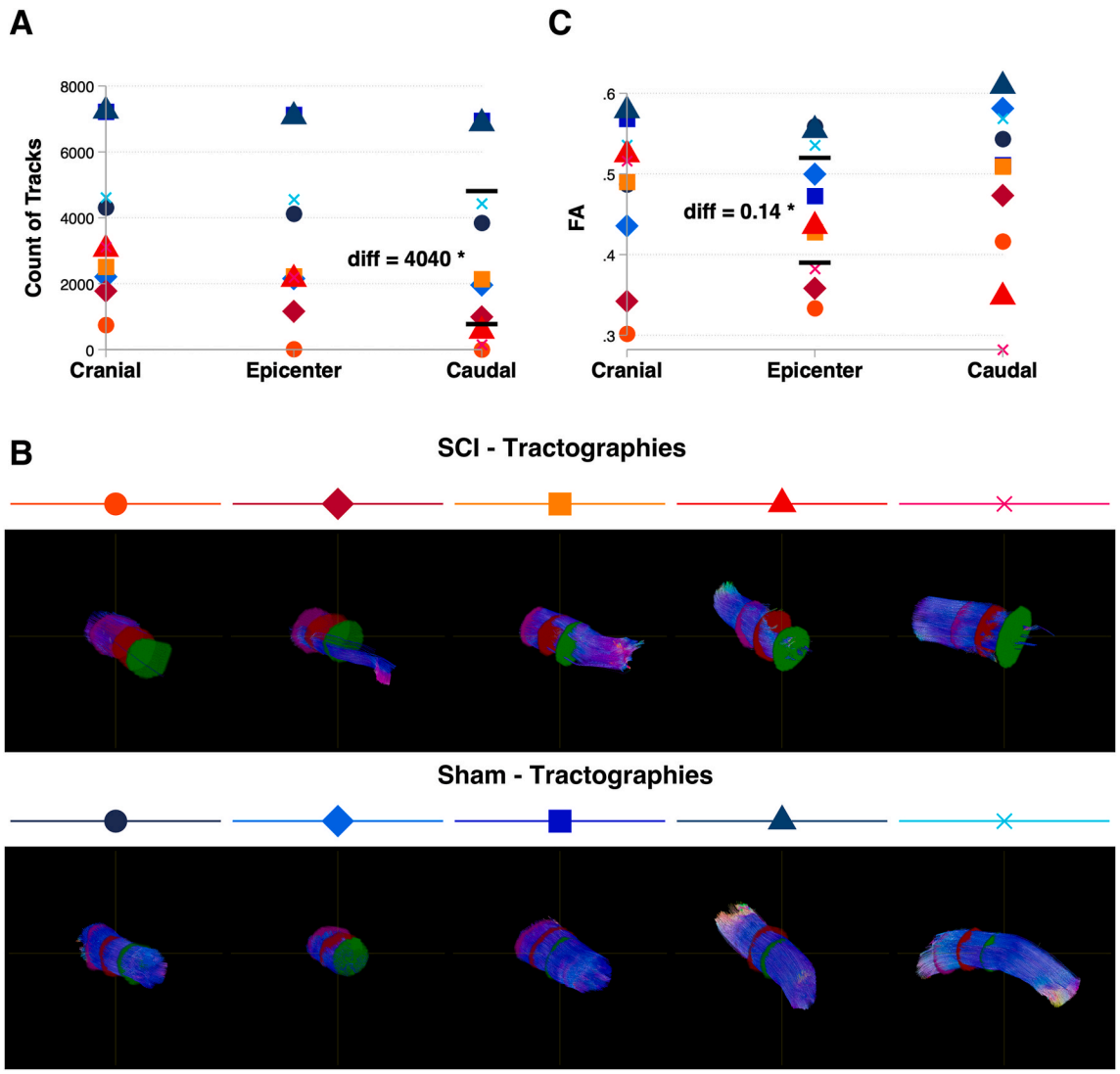

Fig. 2. Results of the MRI-based tractography. Figure illustrating the DTI and tractography analyses for each animal. (**A**) Shows the count of seeded tracks in the purple ROIs (region of interest), and the count of tracks reaching the red (epicenter) and green (caudal end) ROIs. The ROIs are visualized in the 3D tractography in the lower panel (**B**). On the right panel (**B**) the analysis of the mean fractional anisotropy (FA) is shown (same color coding of ROIs). The lower panel shows the individual tractographies and the ROI placement. The symbol annotation and color for each animal in the graphs **(A and C)** is given above each tractography. Black lines: mean for each group. Asterix: significant difference. Blue colors: Sham animals. Red colors: TSCI animals. Purple ROI: seeding point at the cranial end of injury. Red ROI: epicenter of injury. Green ROI: caudal end of the injury.

sham group and 0.39 [0.33, 0.44] for the TSCI group, resulting in a mean difference of 0.14 [0.09, 10.19] and reached statistical significance ($p < 0.000$) (Fig. 2C).

3.2. Histology

One animal was excluded from this analysis, due to cutting artifacts. This was the same animal that was not scanned for DTI, and hence only ten animals were eligible for histological analysis. In all five TSCI animals, the injury was visible by Nissl stain (Fig. 3A).

There were no visible injuries in the Nissl-stained sections of the sham group animals (Fig. 3A). Injury was visible by areas of decreased Nissl staining (n = 5) (Fig. 3A), hemorrhage (n = 5) and/or disintegration (n = 2) of the impact zone (Fig. 3B). In two TSCI animals a lack of nuclei was visible, even when the white matter was intact and without decreased staining, supporting the view of central secondary injury (Fig. 3C).

The injury to total area ratio was below 1 in all sections, meaning that no sections in the TSCI group had signs of complete injury (min: 0, max: 0.86). The mean ratio by each animal was 0.30 [0.16, 0.43] (Fig. 3A).

Visible signs of incomplete injury or necrosis were observed in 94% of the total amount of TSCI sections, suggesting that the injuries had a larger cranio-caudal extent than the impact zone itself.

As for the IBA1 staining, no sham animals demonstrated increased staining in the white or grey matter. In all TSCI animals (n = 5), an increased staining around and of the grey matter was found, suggestive of microglial activation in these parts of the spinal cord (Fig. 3A).

3.3. Physiological stability

Only plasma sodium differed significantly between the TSCI and sham groups (sham 1.8% TSCI 24%, difference: 22.2% p = 0.025) (Table 2). Heart rate (HR), MAP, pH and arterial oxygenation (pO2) were within the reference range for the majority for the study (Fig. 3D–G). However, we observed immediate tachycardia and hypertension following TSCI. The tachycardia diminished during the first hours after injury (Fig. 3D). Some animals were hypoventilated upon

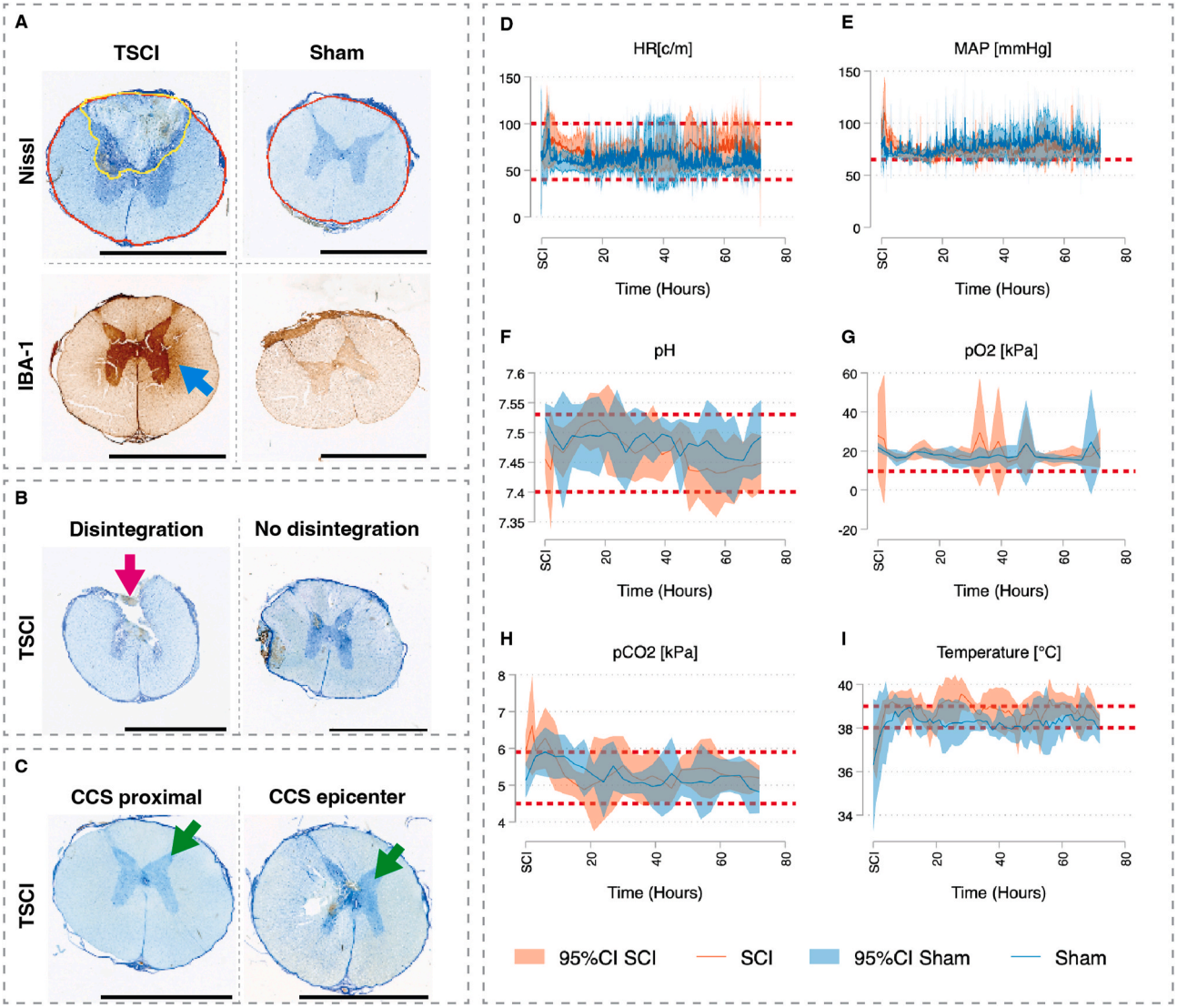

Fig. 3. Results of the histological analysis and physiological parameters. (**A**): Upper: Nissl-stained TSCI and sham sections showing signs of injury to the dorsal part of the spinal cord, by decreased staining (yellow area). No signs of injury can be appreciated in the sham sections. Lower: IBA-1 stained TSCI and sham sections showing central increased staining, suggestive of microglial activation (cyan arrow). The IBA-1-stained section from uninjured sham animal displays no signs of glial activation. Red ROI: is the ROI marking the entire section area. Yellow ROI: The area with decreased staining, corresponding to the injured zone. The injury to total ratio is computed by dividing the two. (**B**) Two sections from different animals illustrating the heterogenicity in injuries. On the left the spinal cord is disintegrated corresponding to the impact zone (magenta arrow). On the right the spinal cord is intact corresponding to the impact zone. (**C**) Two sections from the same animal, illustrating grey matter cell loss, corresponding to central cord syndrome. On the left, a section proximal to the impact zone, displaying grey matter cell loss, assessed by a lack of stained nuclei (green arrow). On the right a section in the impact zone, displaying even more pronounced loss of nuclei (green arrow). For all histological panels, black scale bar = 5000 μm. (**D-I**) Mean (line) and 95% confidence intervals (range) of various physiological parameters measured during the 72 h. Red dashed lines indicate reference values.

arrival, but pCO2 was normalized during the first hours (Fig. 3H). Many animals developed fevers. Especially the TSCI group had an increase in body temperature compared to the sham group (Fig. 3I).

4. Discussion

In this study, we succeeded in producing an incomplete injury, whilst sham animals remained uninjured. Second, we established a protocol for keeping pigs sedated for 72 h, after being subjected to TSCI, while keeping their physiological parameters within normal ranges.

The presented TSCI model differs from previously presented models, particularly on the prolonged (72 h) sedation period following the onset of TSCI.

Falling height and weight of the rod was chosen based on a study which examined the hindlimb function, following various weight drop regimes (Lee et al., 2013). We aimed for an incomplete injury in the range of 4–9 points on the "The Porcine Thoracic Injury Behavioral Scale" (PTIBS) (Lee et al., 2013), which would correspond roughly to an American Spinal Cord injury Association Impairment Scale C-D in human patients (Rupp et al., 2021). The authors of the PTIBS found a regime with a 50 g rod falling at 10 cm would produce impairment in that range (Lee et al., 2013). For manufacturing reasons, we opted for a slightly heavier weight (75 g), whilst decreasing the falling height (75 mm), corresponding to an additional 0.01 J of energy. The group behind PTIBS has published multiple studies in their model and decided upon adding weight (+100 g) to the rod, during the 5 min of compression. We decided against, as we would rather have less than more impairment. Furthermore, they have developed a sophisticated system that does allow for invasive and continuous measurements of intra spinal pressure and micro dialysis even whilst having the animals awaken and moving

Table 2
Mean values of physiological parameters and the proportion of measurements outside the reference range, by group. Mean: the group mean of the mean of each animal. SD: standard deviation. Abnormal: The mean fraction of measurements for each animal, outside the reference range. Test: bootstrapped *t*-test of the mean fractions the abnormal fractions between groups. MAP: Mean arterial pressure, HR: Heart rate, Hgb: hemoglobin.

	Sham				SCI				
	Mean	SD	Abnorm (%)	SD	Mean	SD	Abnorm (%)	SD	Test abnorm (p-value)
MAP [mmHg]	77.50	6.37	5.25	4.71	74.93	3.65	7.23	9.21	0.636
HR [c/m]	61.30	5.04	5.57	7.96	70.79	15.36	10.25	16.52	0.516
Temperature [°C]	38.22	0.38	38.32	15.02	38.77	0.41	53.23	19.01	0.132
pH	7.48	0.03	21.42	9.28	7.46	0.02	21.95	14.52	0.939
pO2 [kPa]	18.46	2.23	1.48	3.31	19.07	2.05	0.00	0.00	0.304
pCO2 [kPa]	5.27	0.20	19.42	13.22	5.42	0.23	25.06	16.69	0.512
glucose [mmol/L]	4.81	0.22	5.87	2.46	4.96	0.54	9.86	12.79	0.443
Hgb [mmol/L]	5.52	0.40	8.73	6.39	5.32	0.68	23.73	30.91	0.231
Sodium [mmol/L]	140.37	0.65	1.79	2.45	141.60	1.75	24.10	25.29	0.025
Potassium [mmol/L]	3.85	0.09	9.76	6.79	3.88	0.19	9.27	7.67	0.906
Chloride [mmol/L]	106.55	1.25	0.00	0.00	106.99	3.04	0.62	1.51	0.300
Urine output 1 h [mL]	93.42	12.64	64.46	5.33	85.82	13.52	67.75	6.08	0.318

around (Streijger et al., 2017, 2021). Keeping the animals sedated facilitated physiological measurements without influences from movements or general animal behavior. A prolonged sedated TSCI model also allows control of blood pressure, ventilation positioning, analgesia, etc.

Another published model applied a hemi-transection of the spinal cord, producing a model of Brown-Sequard Syndrome (Cerro et al., 2021). This model exploits the fact, that the healthy side of the animal can act as its own control but might lack some of the translational traits of a contusion trauma.

A sedated TSCI model disallows neurological examination, which in turn would be the prime outcome measure for intervention studies. Second, the animals are under the influence of propofol, which could affect measures in future intervention studies. From traumatic brain injury (TBI) it is known that sedation can reduce intra-cranial pressure and is considered a therapeutic (Hawryluk et al., 2020). Whether this mechanism also holds true for TSCI is unknown. However, it has been suggested that sevoflurane does not decrease ISP(Werndle et al., 2014). If sedation had a physiological impact in the spinal cord it would most likely be through hypoperfusion, due to anesthetic imposed hypotension. In the current model, hypotension is treated rigorously. Third, to keep the animals stable, we would intervene on physiological parameters as described. This option mimics the clinical situation very well, in which the intensive care doctors and nurses would do the same, but also may mask the potential effects of the TSCI itself.

Our secondary aim was to keep the animals sedated whilst maintaining their physiological measures within normal ranges. In general, animals were kept within these limits, and all animals completed the 72 h of sedation. However, we observed a deviation from normal physiology especially in the first hours after onset of TSCI. An unexpected initial rise in blood pressure was observed in all TSCI animals, being the opposite of the expected neurogenic shock (Ryken et al., 2013). However, over the course of hours, all animals would start to become hypotensive, and require norepinephrine to maintain MAP above 65 mmHg. Similar observations have been made earlier (Guha et al., 1988). It has been found that hypotension is more pronounced in a higher thoracic injury model, which in turn could explain some of our findings (West et al., 2020a). The initial rise in MAP did not respond to increased sedation or analgesia, and hence was not a matter of insufficient sedation, and was probably caused by sympathetic activation. Furthermore, the temperature increased during the experiments. The animals must be considered at high risk for infection. Despite working sterile and administering a prophylactic antibiotic, we failed in keeping animals normothermic. Although temperature rise is well known in TSCI patients following trauma (Savage et al., 2016), we cannot exclude that some animals were infected. TSCI animals spent a significant larger proportion of time outside the reference range with regards to plasma sodium. This was most likely caused by large volume requirement due to neurogenic shock following TSCI.

We found that animals would require increasing infusion rates during the experiments. Constant clinical assessment of sedation and titration was needed, to ensure balanced sufficient sedation.

MRI-based DTI has been used extensively in pre-clinical research, especially in cerebral injuries and in anatomical studies (Stenberg et al., 2021; Næss-Schmidt et al., 2017; Martin et al., 2016; Grossman et al., 2012). The modality has reached well-established clinical use in stroke, where derived metrics, such as the apparent diffusion coefficient is used (van Everdingen, 1998). Furthermore, it has been suggested as a potential diagnostic tool in TSCI (Shanmuganathan et al., 2008, 2017). The tractography produces several tracks, which can be quantitively evaluated. A derived metric is the FA value. FA describes the anisotropy of the diffusion of water molecules, where a value of 0 indicates that diffusion is unrestricted in all directions, and 1 indicates that diffusion is restricted to a single direction. In turn, it is hypothesized that the metric will be sensitive to disruptions in the axonal tracts (Cohen-Adad et al., 2011, 2021).

The DTI algorithm is dependent pre-set parameters, such as the FA threshold. Setting the FA-threshold at a too low value would result in the algorithm being too permissive, whereas a too high value, would be too restrictive. Studies apply different thresholds, usually around 0.1–0.3 (Lundell et al., 2013; Martín et al., 2020). In our study, we decided to determine a reference range for normal FA values in the white matter, by computing the lower bound of the 95% prediction interval for each sham animal and then using the mean of those values. The 95% prediction interval is often used when determining the reference range for biomarkers. By setting the threshold by the method described, the algorithm will, statically, in 97.5% of the cases accept the FA value of uninjured tissue, ensuring that these tracks are permitted to continue. Despite this method, the tracks are only surrogates of neuronal tracts, and whether they represent functional tracts, must be confirmed by future studies in awake animals.

We found that histological analyses supported the results from the MRI-based DTI measurements, that the spinal injury was incomplete and sham animals had intact spinal cords. We found that the injury on average over the sample, would affect approximately 30% of the cord. This is comparable to what was seen in the study by Lee et al. (2013).

Histology is widely used as an ex-vivo modality in animal models and has similarly been applied in various animal models of TSCI(Cerro et al., 2021; Diaz Quiroz et al., 2014). One aim of the histology was to confirm the presence of injury, which in turn could have been done by various stains. We opted for Nissl-stain, which can visualize necrosis, and in turn, allow for visualization of secondary ischemic injury (Popp et al., 2009; Zaer et al., 2020). We found that sections that did not display signs of direct impact, did show signs of necrosis and cell loss, especially in the grey matter, suggesting that the injury exceeded the impact zone itself.

Likewise, we observed glial activation in the same areas; an indicative of secondary ischemic injury along the cord and could be a valuable tool for the evaluation of future intervention studies in the model, where the aim could be mitigation of secondary injury.

There are, as in the DTI analysis, inherent limitation to the histology, as anatomy and not physiological function is displayed.

Future studies could apply repeated measures such as evoked motor potentials, to further validate our findings of incomplete injury. We did perform evoked motor potentials in a sham and found it to be feasible, however the protocol requires optimization in non-injured animals before being put to use, due to large variance in the responses during repeated measuring. The model proved to be physiology stable. For future studies the model may be applied for long term evaluation of neurology and behavior."

Contemporary research in TSCI has moved towards attempting to apply the principles of TBI, in turn establishing a domain of perfusion physiology within the field (Saadoun et al., 2020; Gee et al., 2022). However, moving towards a focus on perfusion also raises questions regarding the vascular physiology of the spinal cord both in the injured and normal state. In the clinic, maintaining of MAP of more than 85 mmHg is recommended (Hadley et al., 2002). Nonetheless, little is known about the actual effects of MAP elevation on spinal cord perfusion and blood flow. In the physiological state, the spinal cord probably is auto-regulated, hence counteracting MAP elevations (Hickey et al., 1986; Kobrine et al., 1976). However, whether this mechanism applies to the injured state, with a disrupted blood brain barrier, is unknown. A few well-designed studies have attempted to evaluate the use of different vasopressors and even calcium channel blockers and have suggested that spinal cord perfusion can be modulated by such interventions and suggested that outcome might be improved (Streijger et al., 2018b; Gallagher et al., 2019; Guha et al., 1989a, 1989b; Gambardella et al., 1995). To evaluate the changes in flow, multiple modalities have been applied, where some include intraparenchymal probes. Whilst yielding high resolution data, they do disrupt the blood brain barrier, potentially biasing the results. Our model would allow for evaluating the blood flow using modalities such as laser speckle contrast throughout the course of 72 h. As suggested by Gee et al. (2022), further investigation is needed to establish the physiological basis for MAP augmentation and other strategies aiming to increase perfusion.

Strategies such as expansive duroplasty and lumbar drainage are based on the premise that the dural casing maintains a compartment syndrome, leading to hypoperfusion (Phang et al., 2015; Kwon et al., 2009). We find that our model could contribute to such areas, allowing for undisturbed and precise intraspinal monitoring. Finally, studies applying high resolution and real-time in-vivo imaging to examine the swelling of the cord below the dura, and hence non-invasively evaluate the space-occupation would be possible using our model.

5. Conclusion

This study succeeded in producing a porcine model of incomplete TSCI, which was physiologically stable up to 72 h. We believe that this TSCI model will constitute a potential translational model to study the accompanied immunological, regenerative and hemodynamic mechanisms secondary to TSCI in humans.

Authorship confirmation/contribution statement

Mathias Møller Thygesen: Conceptualization, Data curation, Investigation, Formal analsysis, Funding Acquisition, Methodology, Software, Visualization, Writing – Original Draft. Seyar Entezari: Investigation, Writing – review & editing. Nanna Houlind: Investigation, Writing – review & editing. Teresa Haugaard Nielsen: Investigation, Writing – review & editing. Nicholas Østergaard Olsen: Investigation, Writing – review & editing. Tim Damgaard Nielsen: Investigation, Formal analysis, Writing – review & editing. Mathias Skov: Investigation, Writing – review & editing. Alp Tankisi: Supervision, Software, Writing – review & editing. Mads Rasmussen: Supervision, Writing – review & editing. Halldór Bjarki Einarsson: Investigation, Writing – review & editing. Peter Agger: Supervision, Software, Writing – review & editing. Dariusz Orlowski; Investigation, Methodology, Supervision Writing – review & editing. Stig Eric Dyrskog: Supervision, Methodology, Resources, Writing – review & editing. Line Thorup: Supervision, Methodology, Writing – review & editing. Michael Pedersen: Investigation, Supervision, Methodology, Resources, Project administration, Writing – review & editing. Mikkel Mylius Rasmussen: Conceptualization, Investigation, Supervision, Methodology, Resources, Project administration, Funding acquisition, Writing – review & editing.

Authors' disclosure statement

The authors declare that they have no conflicts of interest.

Funding statement

This study was funded by Offerfonden ("The Victims Foundation" under Ministry of Justice of Denmark), The Riisfort Foundataion, AP Møller Mærsk Foundation, The Dagmar Marshalls Foundation and Aarhus University.

Declaration of competing interest

The authors declare the following financial interests/personal relationships which may be considered as potential competing interests:

Mathias Thygesen reports financial support was provided by Offerfonden (Victims Foundation, Ministry of Justice Denmark). Mathias Thygesen reports financial support was provided by The Riisfort Foundataion. Mathias Thygesen reports financial support was provided by AP Møller Mærsk Foundation. Mathias Thygesen reports financial support was provided by The Dagmar Marshalls Foundation.

References

Cerro, P.D., et al., 2021. Neuropathological and motor impairments after incomplete cervical spinal cord injury in pigs. J. Neurotrauma.
Cohen-Adad, J., et al., 2011. Demyelination and degeneration in the injured human spinal cord detected with diffusion and magnetization transfer MRI. Neuroimage 55 (3), 1024–1033.
Cohen-Adad, J., et al., 2021. Generic acquisition protocol for quantitative MRI of the spinal cord. Nat. Protoc. 16 (10), 4611–4632.
Diaz Quiroz, J.F., et al., 2014. Precise control of miR-125b levels is required to create a regeneration-permissive environment after spinal cord injury: a cross-species comparison between salamander and rat. Disease Models & Mechanisms 7 (6), 601–611.
Gallagher, M.J., et al., 2019. Spinal cord blood flow in patients with acute spinal cord injuries. J. Neurotrauma 36 (6), 919–929.
Gambardella, G., et al., 1995. Experimental incomplete spinal cord injury: treatment with a combination of nimodipine and adrenaline. J. Neurosurg. Sci. 39 (1), 67–74.
Gee, C.M., Kwon, B.K., 2022. Significance of spinal cord perfusion pressure following spinal cord injury: a systematic scoping review. J Clin Orthop Trauma 34, 102024.
Grossman, E.J., et al., 2012. Thalamus and cognitive impairment in mild traumatic brain injury: a diffusional kurtosis imaging study. J. Neurotrauma 29 (13), 2318–2327.
Guha, A., Tator, C.H., 1988. Acute cardiovascular effects of experimental spinal cord injury. J. Trauma 28 (4), 481–490.
Guha, A., et al., 1989a. Improvement in post-traumatic spinal cord blood flow with a combination of a calcium channel blocker and a vasopressor. J. Trauma 29 (10), 1440–1447.
Guha, A., Tator, C.H., Rochon, J., 1989b. Spinal cord blood flow and systemic blood pressure after experimental spinal cord injury in rats. Stroke 20 (3), 372–377.
Hadley, M.N., et al., 2002. Management of acute central cervical spinal cord injuries. Neurosurgery 50 (3 Suppl. l), S166–S172.
Hannon, J.P., Bossone, C.A., Wade, C.E., 1990. Normal physiological values for conscious pigs used in biomedical research. Lab. Anim. Sci. 40 (3), 293–298.
Hawryluk, G.W.J., et al., 2020. Guidelines for the management of severe traumatic brain injury: 2020 update of the decompressive craniectomy recommendations. Neurosurgery 87 (3), 427–434.
Hickey, R., et al., 1986. Autoregulation of spinal cord blood flow: is the cord a microcosm of the brain? Stroke 17 (6), 1183–1189.
James, N.D., et al., 2015. Chondroitinase gene therapy improves upper limb function following cervical contusion injury. Exp. Neurol. 271, 131–135.

Kigerl, K.A., et al., 2009. Identification of two distinct macrophage subsets with divergent effects causing either neurotoxicity or regeneration in the injured mouse spinal cord. J. Neurosci. 29 (43), 13435–13444.
Kobrine, A.I., Doyle, T.F., Rizzoli, H.V., 1976. Spinal cord blood flow as affected by changes in systemic arterial blood pressure. J. Neurosurg. 44 (1), 12–15.
Kwon, B.K., et al., 2009. Intrathecal pressure monitoring and cerebrospinal fluid drainage in acute spinal cord injury: a prospective randomized trial - clinical article. J. Neurosurg. Spine 10 (3), 181–193.
Lee, J.H., et al., 2013. A novel porcine model of traumatic thoracic spinal cord injury. J. Neurotrauma 30 (3), 142–159.
Lundell, H., et al., 2013. Fast diffusion tensor imaging and tractography of the whole cervical spinal cord using point spread function corrected echo planar imaging. Magn. Reson. Med. 69 (1), 144–149.
Martin, A.R., et al., 2016. Translating state-of-the-art spinal cord MRI techniques to clinical use: a systematic review of clinical studies utilizing DTI, MT, MWF, MRS, and fMRI. Neuroimage Clin 10, 192–238.
Martín Noguerol, T., et al., 2020. Optimizing diffusion-tensor imaging acquisition for spinal cord assessment: physical basis and technical adjustments. Radiographics 40 (2), 403–427.
Martirosyan, N.L., et al., 2015. Cerebrospinal fluid drainage and induced hypertension improve spinal cord perfusion after acute spinal cord injury in pigs. Neurosurgery 76 (4), 461–468.
Næss-Schmidt, E.T., et al., 2017. Microstructural changes in the thalamus after mild traumatic brain injury: a longitudinal diffusion and mean kurtosis tensor MRI study. Brain Inj. 31 (2), 230–236.
Phang, I.S., et al., 2014. Injured spinal cord pressure evaluation (iscope) study: expansion duroplasty reduces spinal cord pressure in acute spinal cord injury. J. Neurotrauma 31 (5), A28.
Phang, I., et al., 2015. Expansion duroplasty improves intraspinal pressure, spinal cord perfusion pressure, and vascular pressure reactivity index in patients with traumatic spinal cord injury: injured spinal cord pressure evaluation study. J. Neurotrauma 32 (12), 865–874.
Popovich, P.G., et al., 1999. Depletion of hematogenous macrophages promotes partial hindlimb recovery and neuroanatomical repair after experimental spinal cord injury. Exp. Neurol. 158 (2), 351–365.
Popp, A., et al., 2009. Identification of ischemic regions in a rat model of stroke. PLoS One 4 (3), e4764.
Rupp, R., et al., 2021. International standards for neurological classification of spinal cord injury: revised 2019. Top. Spinal Cord Inj. Rehabil. 27 (2), 1–22.
Ryken, T.C., et al., 2013. The acute cardiopulmonary management of patients with cervical spinal cord injuries. Neurosurgery 72 (Suppl. 2), 84–92.
Saadoun, S., Papadopoulos, M.C., 2016. Spinal cord injury: is monitoring from the injury site the future? Crit. Care 20 (1), 308.
Saadoun, S., Papadopoulos, M.C., 2020. Targeted perfusion therapy in spinal cord trauma. Neurotherapeutics 17 (2), 511–521.
Savage, K.E., et al., 2016. Neurogenic fever after acute traumatic spinal cord injury: a qualitative systematic review. Global Spine J. 6 (6), 607–614.
Schindelin, J., et al., 2012. Fiji: an open-source platform for biological-image analysis. Nat. Methods 9 (7), 676–682.
Schomberg, D.T., et al., 2017. Translational relevance of swine models of spinal cord injury. J. Neurotrauma 34 (3), 541–551.
Schwab, J.M., et al., 2014. The paradox of chronic neuroinflammation, systemic immune suppression, autoimmunity after traumatic chronic spinal cord injury. Exp. Neurol. 258, 121–129.
Shanmuganathan, K., et al., 2008. Diffusion tensor MR imaging in cervical spine trauma. AJNR Am J Neuroradiol 29 (4), 655–659.
Shanmuganathan, K., et al., 2017. Diffusion tensor imaging parameter obtained during acute blunt cervical spinal cord injury in predicting long-term outcome. J. Neurotrauma 34 (21), 2964–2971.
Silver, J., Schwab, M.E., Popovich, P.G., 2015. Central nervous system regenerative failure: role of oligodendrocytes, astrocytes, and microglia. Cold Spring Harbor Perspect. Biol. 7 (3), a020602.
Smielewski, P., et al., 2005. ICM+: software for on-line analysis of bedside monitoring data after severe head trauma. Acta Neurochir. Suppl. 95, 43–49.
Squair, J.W., et al., 2019. Empirical targets for acute hemodynamic management of individuals with spinal cord injury. Neurology 93 (12), e1205–e1211.
Stenberg, J., et al., 2021. Acute diffusion tensor and kurtosis imaging and outcome following mild traumatic brain injury. J. Neurotrauma.
Streijger, F., et al., 2017. Changes in pressure, hemodynamics, and metabolism within the spinal cord during the first 7 Days after injury using a porcine model. J. Neurotrauma 34 (24), 3336–3350.
Streijger, F., et al., 2018a. A direct comparison between norepinephrine and phenylephrine for augmenting spinal cord perfusion in a porcine model of spinal cord injury. J. Neurotrauma 35 (12), 1345–1357.
Streijger, F., et al., 2018b. A direct comparison between norepinephrine and phenylephrine for augmenting spinal cord perfusion in a porcine model of spinal cord injury. J. Neurotrauma 35 (12), 1345–1357.
Streijger, F., et al., 2021. Duraplasty in traumatic thoracic spinal cord injury: impact on spinal cord hemodynamics, tissue metabolism, histology, and behavioral recovery using a porcine model. J. Neurotrauma 38 (21), 2937–2955.
Tator, C.H., Fehlings, M.G., 1991. Review of the secondary injury theory of acute spinal cord trauma with emphasis on vascular mechanisms. J. Neurosurg. 75 (1), 15–26.
Thygesen, M.M., et al., 2021. A review of spinal cord perfusion pressure guided interventions in traumatic spinal cord injury. Eur. Spine J. 30 (10), 3028–3035.
Tournier, J.D., et al., 2019. MRtrix3: a fast, flexible and open software framework for medical image processing and visualisation. Neuroimage 202, 116137.
van Everdingen, K.J., et al., 1998. Diffusion-weighted magnetic resonance imaging in acute stroke. Stroke 29 (9), 1783–1790.
Weber-Levine, C., et al., 2022. Porcine model of spinal cord injury: a systematic review. Neurotrauma Rep 3 (1), 352–368.
Werndle, M.C., et al., 2013. Measurement and optimisation of spinal cord perfusion pressure in acute spinal cord injury. Br. J. Neurosurg. 27 (5), 556.
Werndle, M.C., et al., 2014. Monitoring of spinal cord perfusion pressure in acute spinal cord injury: initial findings of the injured spinal cord pressure evaluation study. Crit. Care Med. 42 (3), 646–655.
West, C.R., et al., 2020a. A porcine model for studying the cardiovascular consequences of high-thoracic spinal cord injury. Journal of Physiology-London 598 (5), 929–942.
West, C.R., et al., 2020b. A porcine model for studying the cardiovascular consequences of high-thoracic spinal cord injury. J Physiol 598 (5), 929–942.
Zaer, H., et al., 2020. Radionecrosis and cellular changes in small volume stereotactic brain radiosurgery in a porcine model. Sci. Rep. 10 (1), 16223.
Zorner, B., Schwab, M.E., 2010. Anti-Nogo on the go: from animal models to a clinical trial. Ann. N. Y. Acad. Sci. 1198 (Suppl. 1), E22–E34.